Atmósfera 40, 167-187 (2026)
https://doi.org/10.20937/ATM.53535

Synoptic patterns associated with heavy rainfall events in the western and southwestern mesoregions of Paraná State, Brazil

Gustavo Carlos Juan ESCOBAR*, Marcelo BARBIO ROSA and Carlos Renato DE SOUZA

Instituto Nacional de Pesquisas Espaciais (INPE), 12630-000, Cachoeira Paulista, SP, Brasil.
*Corresponding author: gustavo.escobar@inpe.br

Received: September 23, 2025; Accepted: January 6, 2026

RESUMEN

Este estudio presenta una clasificación sinóptica de eventos de lluvia intensa en las mesorregiones occidental y suroccidental del Estado de Paraná entre 2000 y 2022. Se identificó un total de 178 casos, caracterizados por acumulaciones diarias de precipitación que superaron los 32.8 mm. La clasificación identificó cuatro patrones sinópticos principales asociados a los eventos de lluvia intensa en la región de estudio. Dos de estos patrones estuvieron vinculados al paso de un frente frío, mientras que los otros dos se relacionaron con procesos ciclogenéticos. Los cuatro patrones mostraron, en superficie, vientos del noroeste que comenzaron dos días antes de la ocurrencia de los eventos de lluvia intensa. Las depresiones del Noroeste Argentino y del Chaco fueron identificadas como los principales sistemas meteorológicos que transportan aire cálido y húmedo hacia la región de estudio. Los cuatro patrones sinópticos mostraron el desarrollo de sistemas convectivos iniciados un día antes de la ocurrencia de los eventos de lluvia intensa en la región de estudio. Entre ellos, el patrón sinóptico asociado con un frente frío con desplazamiento zonal mostró la actividad convectiva más intensa alrededor de la región de estudio, según lo indicado por temperaturas de luminosidad inferiores a 240 K. El patrón sinóptico asociado con ciclogénesis y con una configuración de bloqueo mostró circulación ciclónica en superficie desde el día anterior a la ocurrencia de los eventos de lluvia intensa, lo que provocó una mayor convergencia de masa en superficie. Este mecanismo contribuyó a intensificar las lluvias en la región de estudio, destacando el rol de la vorticidad a bajos niveles en el mantenimiento de la precipitación intensa.

ABSTRACT

This study presents a synoptic classification of heavy rainfall events in the western and southwestern mesoregions of Paraná State between 2000 and 2022. A total of 178 cases were identified, characterized by daily precipitation accumulations exceeding 32.8 mm. The classification revealed four principal synoptic patterns associated with heavy rainfall events in the study region. Two of these patterns were linked to the passage of a cold front, while the remaining two were tied to cyclogenetic processes. All four patterns exhibited northwesterly winds at the surface level beginning two days prior to the occurrence of the heavy rainfall event. The Northwestern Argentinean Low and Chaco Low were identified as the main meteorological systems that advect warm, moist airflow into the study region. All four synoptic patterns showed the development of convective systems starting one day before the occurrence of a heavy rainfall event in the study region. Among them, the synoptic pattern associated with a cold front featuring a zonal displacement exhibited the most intense convective activity around the study region, as indicated by brightness temperatures below 240 K. The synoptic pattern associated with cyclogenesis and with a blocking configuration showed surface cyclonic circulation as early as the day before the occurrence of the heavy rainfall events, leading to increased surface mass convergence. This mechanism contributed to intensified rainfall in the study region, underscoring the role of low-level vorticity in sustaining heavy precipitation.

Keywords: synoptic climatology, heavy rainfall, cold front, cyclogenesis.

1. Introduction

The heavy rainfall events (HRE) that occur in the State of Paraná (PR) are driven by synoptic and sub-synoptic-scale meteorological systems that act on a large part of the southern region of Brazil throughout the year. Examples include cold fronts (Andrade, 2005; Cavalcanti and Kousky, 2009; Foss et al., 2017), baroclinic troughs (Escobar et al., 2019a), upper-level cyclonic vortices (Reboita et al., 2010a), and extratropical and subtropical cyclones (Taljaard, 1972; Simmonds and Keay, 2000; Hoskins and Hodges, 2005; Reboita et al., 2010b; Gozzo et al., 2014).

According to the State of PR's civil defense, half of the natural disasters that occurred between 1990 and 1999 were caused by HREs. These events had significant impacts, including floods, waterlogging, flash floods, and mass movement (Balicki et al., 2020).

The southern region of Brazil is characterized by one of the highest frequencies of severe storms in the country, which can be accompanied by tornadoes (Dyer, 1994; Silva, 2011; Balicki et al., 2020) and, in many cases, lead to HRE.

According to Zipser et al. (2006), the western and southwestern mesoregions (WSM) of the State of PR, along with the northwest of the State of Rio Grande do Sul (RS), the west of Santa Catarina (SC), the southeast of Paraguay, and the northeast of Argentina, are among the regions with the strongest storms in the world.

These regions are affected by frequent mesoscale convective complexes (MCCs) (Maddox, 1980; Velasco and Fritsch, 1987) that mainly act during summer and transitional seasons, causing HRE and significantly contributing to annual precipitation totals (Rasmussen et al., 2016).

MCCs intensify from the interaction of the upper-level subtropical jet with the low-level jet (LLJ) that advects warm and humid air from the north (Marengo et al., 2004; Salio et al., 2007; Castañeda and Ulke, 2015; Dos Santos and Reboita, 2018; Montini et al., 2019; Moraes et al., 2020). The LLJ is strengthened by the presence of the Chaco Low (CHL) and the Northwestern Argentinean Low (NAL), located approximately between central-northern Argentina, southern Bolivia, and western Paraguay (Seluchi et al., 2003; Escobar and Seluchi, 2012; Marengo et al., 2012). Depending on the position of both low-pressure systems, the LLJ is directed towards the western portion of the southern region of Brazil, including the WSM of PR. Therefore, the warm and humid air from the Amazon region favors an increase in low-level moisture potential, which contributes to atmospheric destabilization, being one of the necessary ingredients for severe storms.

According to Teixeira and Satyamurty (2007), the main conceptual model associated with the occurrence of HRE in the southern region of Brazil is related to four relevant characteristics: (i) the intensification of a trough in the middle troposphere in the eastern Pacific Ocean that approaches the continent three days before the occurrence of the HRE; (ii) the presence of a low-pressure system centered in northern Argentina (NAL or CHL) one day before the occurrence of the HRE; (iii) the development of the LLJ over Paraguay two days before the occurrence of the HRE; and (iv) a strong convergence of moisture flow over the southern region of Brazil one day before the HRE episode.

Bugoni et al. (2018) and Ferreira et al. (2022) analyzed two severe weather events in the WSM of PR, both occurring in 2015 and driven by similar synoptic setups. The first, an HRE on September 7, produced 136.3 mm in one hour in Foz do Iguaçu—equivalent to 20% of September's monthly average—while the second, a multiple-vortex tornado on November 19, impacted Marechal Cândido Rondon, injuring 31 people and causing ~\$16.5 million in damages. In both cases, the primary synoptic drivers were a 500 hPa trough and the presence of the NAL, which enhanced LLJ intensity and provided the necessary dynamics for extreme convection. These studies highlight the critical role of the synoptic-scale systems in triggering severe mesoscale phenomena in the region.

Despite the high frequency and significant socioeconomic impacts of HRE in the WSM of the State of PR, the synoptic circulation patterns that influence their occurrence remain poorly documented. Most existing studies on HRE in this region focus either on synoptic analysis of individual case studies or on statistical assessments of average meteorological conditions. However, there is a lack of objective research that systematically examines the variability around these mean synoptic conditions.

Investigating this variability is crucial for identifying the dominant synoptic patterns linked to HRE in the WSM of PR, which will also help meteorologists improve their forecasts and minimize the impacts of these heavy flooding and landslide events in vulnerable regions. In this sense, Escobar and Barbio (2024) elaborated a synoptic climatology of HRE in the metropolitan region of Porto Alegre (RS). According to the authors, the CHL and the NAL played a decisive role in intensifying the LLJ, which contributes to enhanced rainfall in the study area.

Therefore, the main objective of this work is to study the variability of atmospheric circulation at the surface and at altitude by elaborating a synoptic classification associated with the occurrence of HRE in the WSM of the State of PR.

This paper is organized as follows: section 2 details the data and methodology used in this study; section 3 identifies the main synoptic patterns associated with HRE in the study area, and section 4 presents the conclusions.

2. Data and methodology

2.1 Data

To detect the HRE in the WSM, daily precipitation data from 2000 to 2022 were utilized. This data was sourced from the MERGE product (Rozante et al., 2020), which offers a spatial resolution of 0.1º × 0.1º. The MERGE product is a composite dataset that integrates surface observations across the South American continent with precipitation estimates from the Tropical Rainfall Measuring Mission (TRMM) satellite. The observed data used in the MERGE product underwent INPE's operational quality control system, which consists of two stages, as described in Rozante et al. (2018).

To study the synoptic features linked with HRE in the WSM, we utilized daily meteorological data at 12:00 UTC from the National Centers for Environmental Prediction (NCEP) Climate Forecast System Reanalysis (CFSR) for the years 2000-2022. The CFSR v. 1 (Saha et al., 2010) encompasses the period from January 1979 to March 2011, while CFSR v. 2 (Saha et al., 2014), which was introduced in March 2011, has been operational since then. Both versions have a horizontal native resolution of T382 (~38 km). Their horizontal resolution is set at 0.25º × 0.25º between 10º S and 10º N, gradually decreasing towards the poles, reaching 0.5º between 30º N and 30º S.

Although ERA5 (European Centre for Medium-Range Weather Forecasts Reanalysis 5) (Hersbach et al., 2020) is a more recent, higher-resolution dataset, the lower-resolution CFSR data were chosen in this case to reduce computational demands when applying the statistical methodology used to study synoptic-scale variability. Moreover, since this study focuses on synoptic-scale meteorological systems, the CFSR data's resolution is already sufficient to identify them.

We selected the 12:00 UTC datasets because this time provides a higher density of observations over the South American continent, leading to more accurate analysis. The meteorological variables from the CFSR that were used include: (i) mean sea level pressure (SLP) in hPa; (ii) specific humidity at 850 hPa (q850) in g kg^{-1}; and (iii) geopotential height at 500 hPa (GH500) in gpm, all for the period 2000-2022.

In addition, images captured by the Geostationary Operational Environmental Satellite (GOES) series, particularly those in the thermal infrared (IR) channels (Knapp et al., 2011), were obtained at a spatial resolution of 0.1º at 12:00 UTC. These GOES images were instrumental in identifying the cloud patterns associated with HRE in the WSM.

However, it is important to acknowledge a key limitation: satellite imagery at 12:00 UTC does not capture the full diurnal cycle of convective development. Convective systems typically intensify in the afternoon, when diurnal heating becomes a dominant driver. Despite this constraint, the 12:00 UTC time was prioritized due to the greater observational coverage and resulting data reliability at this synoptic hour.

2.2 Identification of HRE

Various criteria exist for identifying HRE, which may take into account factors such as the volume of rain recorded within a specific time frame and the geographical extent of this rainfall, or just one of these parameters (Teixeira and Satyamurty, 2007). Some research has employed climatology to define HRE (Liebmann et al., 2001; Carvalho et al., 2002). As the focus of this study is to identify the synoptic patterns associated with the onset of HRE rather than its persistence, only the first day of HRE is considered.

In our study, we selected HRE using the percentile technique (Dereczynski et al., 2009; Da Silva and Reboita, 2014; Escobar et al., 2016). This method involved calculating daily precipitation quantiles based on the average precipitation in a chosen area (box in Fig. 1), utilizing MERGE rainfall data with a spatial resolution of 0.1º × 0.1º. The WSM of PR are contained within the box in Figure 1b.

In the specified region, rainfall values exceeding the 95th percentile (a daily precipitation value that separates the highest 5% of the daily precipitation data from the remaining 95%) were considered, corresponding to accumulations greater than 32.8 mm per day. The choice of the 95th percentile was primarily based on the fact that it is the threshold most commonly used in the literature for identifying episodes of intense daily rainfall. Moreover, using this threshold allowed for the selection of an adequate number of events, thereby enhancing the statistical robustness of the results. A test was also conducted using the 99th percentile; however, the number of resulting cases was very low—fewer than 50.

A larger area (box), which encompasses the WSM, was utilized because the primary objective of this paper is to examine synoptic-scale features associated with HRE and exclude those caused by isolated small-scale atmospheric perturbations.

2.3 Synoptic classification

Based on the selection criteria for HRE in the WSM (as outlined in section 2.2), a total of 178 cases were identified for the period spanning from 2000 to 2022. Each case represents a day with daily precipitation exceeding 32.8 mm. A synoptic classification of these events was then conducted using the principal pattern sequence analysis (PPSA) method (Compagnucci et al., 2001; Escobar et al., 2004; Huth et al., 2008). The study area is defined by the coordinates 5º to 40º S and 30º to 80º W (Fig. 2a).

According to Compagnucci et al. (2001), PPSA can be seen as an extension of the traditional principal component analysis (PCA), utilizing a correlation matrix in T-mode (Green and Carrol, 1978; Richman, 1986; Escobar et al., 2016).

PCA is valuable for identifying distinct types of atmospheric flow. However, PPSA goes further by classifying sequences of circulation patterns, thereby enabling a more comprehensive understanding of the life cycle of synoptic systems—including cyclogenesis and anticyclogenesis, their trajectories, evolution, and dissipation. The primary objective of PPSA is to identify the dominant modes of system evolution, facilitating the study of the tracks and behavior of synoptic-scale systems within a specific region.

T-mode PPSA is applied to analyze spatial fields across different time steps. In this approach, each

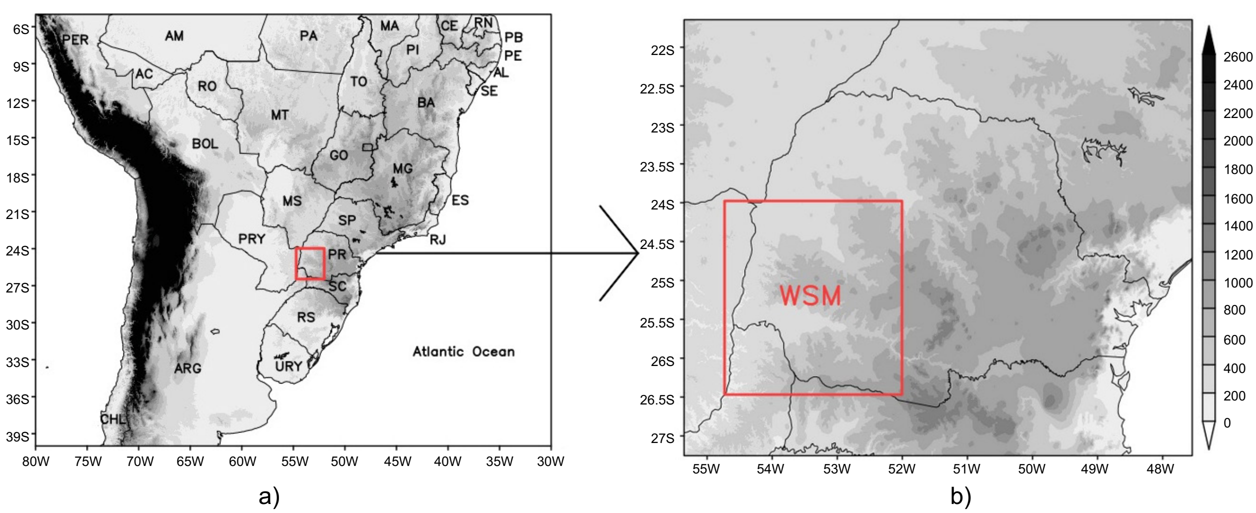

Fig. 1. (a) Area selected for study. The red box shows the western and southwestern mesoregions (WSM) of the State of Paraná; (b) grid of the merged rainfall data within the area selected. Shaded areas represent orography in meters.

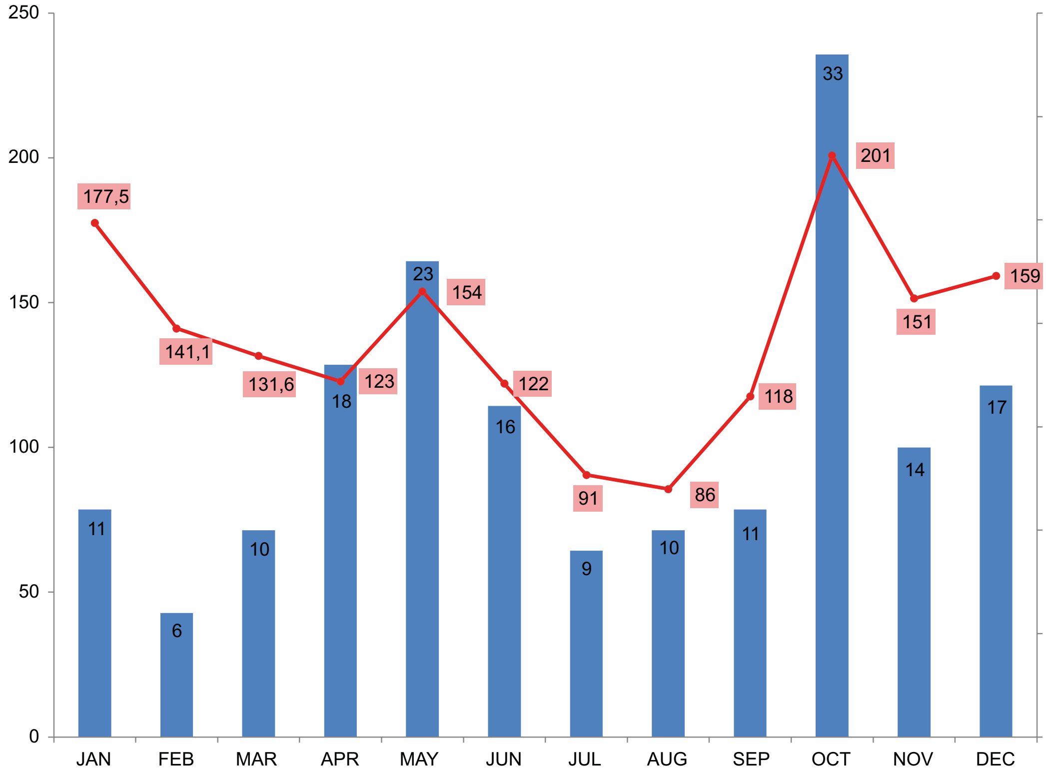

Fig. 2. Monthly frequency of the number of cases of HRE in the WSM, during 2000-2022 (blue columns) and monthly precipitation climatology (2000-2022) (red line). (HRE: heavy rainfall events; WSM: western and southwestern mesoregions of the State of Paraná).

variable is a sequence of the consecutive spatial fields of a given meteorological variable, and observations correspond to grid points. This allows the method to identify and isolate subgroups of fields that share a similar spatial structure. T-mode analysis facilitates the identification of recurrent synoptic situations, strengthening the fundamental knowledge required for weather forecasting.

The matrices used have dimensions of 178 × 7171 (days × grid points) for two days prior to the occurrence of HRE in the WSM (Day –2), one day before the occurrence of HRE in the WSM (Day –1), and on the day of the HRE occurrence in the WSM (Day 0). Thus, the cases correspond to 178 days, while the variables are the selected grid points over the domain (7171). The final input matrix for the PPSA has dimensions of 178 × 21 513 (days × grid points). Because we are using T-mode, this matrix is constructed by vertically concatenating three individual matrices (i.e., stacking them one below the other). The PPSA was executed separately for each meteorological field (SLP, GH500, and q850).

Following the application of PPSA, Varimax rotation (Richman, 1986) was performed. This technique helps redistribute the total variance among the components, thereby enhancing the physical significance of the generated principal pattern sequences (PPSs) (Richman, 1986). The ideal number of rotated PPSs was determined using the eigenvalue 1.0 rule (Richman et al., 1992).

Significant correlations between real meteorological fields and the PPSs were identified through time series of factor loadings. These loadings represent the correlations between the variable used (real meteorological field) and each PPS (Richman, 1986). Analyzing the factor loadings enables the evaluation of the representative patterns (derived from PPSA) as actual atmospheric circulation fields (recorded in the reanalysis). Factor loading values closer to 1 indicate sequences of atmospheric circulation fields that closely resemble the obtained pattern sequence (Harman, 1976; Cattell, 1978).

Richman and Gong (1999) emphasize the critical importance of carefully selecting an appropriate cutoff loading value for meteorological analyses. Extremely high thresholds (e.g., 0.7) risk discarding meaningful physical signals embedded in the data, resulting in incomplete or biased interpretations. Conversely, thresholds near zero risk fail to reliably capture pattern signals.

The authors recommend that acceptable loading values typically fall within the range of 0.2-0.4. However, in this study, a cutoff of 0.6 was adopted to identify significant loadings, balancing the need to retain physically relevant signals while avoiding excessive noise in the analysis. PPSs can be analyzed in both their positive and negative phases (Compagnucci and Salles, 1997). Each PPS corresponds to two distinct synoptic patterns with identical spatial configurations but opposite sign conventions. In the direct mode (positive factor loadings), the PPS shares the same sign as the meteorological variable under analysis. For example, positive (negative) values of SLP in a PPS indicate high (low) pressure systems. Conversely, in the indirect mode (negative loadings), this relationship is inverted: positive (negative) PPS values correspond to low (high) pressure systems.

In this study, significant factor loadings were predominantly positive, indicating that the PPS directly corresponded to observed meteorological conditions (e.g., weather types such as high- or low-pressure systems). This alignment ensures that the derived patterns reflect the actual atmospheric states rather than inverse configurations.

To investigate the synoptic variability of the entire troposphere associated with HRE in the WSM of PR, PPSs were analyzed across three atmospheric levels: the surface, 850 hPa, and 500 hPa. The analysis began with a subjective visual examination of PPS at each level, informed by synoptic knowledge of South America's atmospheric dynamics and forecasting expertise. Given the baroclinic vertical structure characteristic of many HRE-linked weather systems (Lackmann, 2015), this approach enabled rapid identification of vertical connections among atmospheric layers.

To validate these visual interpretations, an objective method was applied: linear correlations (Pearson r) (Kutner et al., 2005) were calculated between the time series of factor loadings for each identified PPS across all three levels. This step ensured consistency between subjective pattern recognition and statistically derived relationships among atmospheric layers. A similar approach was applied by Escobar (2019, 2023) and Escobar and Reboita (2022) when they made a synoptic climatology of SACZ episodes and synoptic classification of the rainy season and winter in Brazil, respectively.

Lastly, the seasonal contribution of each surface-level PPS was evaluated by calculating the variance it explained during different seasons. This was achieved using the factor loading time series (considering loadings greater than 0.6) (Harman, 1976; Cattell, 1978), which allowed for an assessment of how the influence of each PPS varied across the seasonal cycles.

Following the synoptic classification of atmospheric patterns associated with HREs in the study region, we generated composite fields for thermal infrared imagery and mean SLP. These composites were derived from cases assigned to each surface-level PPS that exhibited strong pattern representation, defined by factor loadings ≥ 0.6 (Richman and Gong, 1999). The composite fields were constructed for Day –2, Day –1, and Day 0.

3. Results and discussion

3.1 Synoptic patterns associated with HRE in the WSM

Figure 2 illustrates the monthly distribution of HRE in the WSM and the associated monthly precipitation climatology. Both datasets show synchronized seasonal patterns, with the highest HRE frequencies occurring in May (23 cases) and October (33 cases). This alignment is likely driven by favorable thermodynamic conditions, which, when coupled with baroclinic atmospheric dynamics, intensify rainfall intensity (Escobar et al., 2016).

The reduced HRE frequency observed during January, February, and March is probably linked to diminished baroclinic activity, even though humidity levels remain elevated during this period. Conversely, the observed minimum in HRE occurrences during July, August, and September coincides with lower atmospheric moisture availability.

This contrast underscores the critical role of synoptic-scale atmospheric interactions, specifically the interplay between moisture supply and baroclinic systems, in governing both the intensity and frequency of HRE.

Table I shows the percentage of explained variance (P. Var) and cumulative percentage of explained variance (C.P. Var) for the retained PPSs of the three meteorological variables: GH500, SLP, and q850.

The synoptic classification at the 500 hPa level (GH500), associated with HRE in the WSM, identified six PPSs that collectively explain 94.4% of the total variance (Table I).

The temporal series of factor loadings linked to the first four PPSs predominantly exhibit positive values, with several exceeding the 0.6 threshold. This suggests that these PPSs closely resemble real-world weather patterns, as their configurations align with observed atmospheric conditions. The remaining PPSs, while representing valid meteorological scenarios, are excluded from this analysis because their factor loadings fall below the 0.6 cutoff—a criterion established by Harman (1976) and Cattell (1978) to ensure statistically significant physical relevance.

At the surface (SLP), six PPSs were identified, explaining 77.3% of the total variance (Table I). The first four PPSs alone account for 64.6% of this variance. Most factor loading values for these PPSs are positive, with many exceeding the 0.6 threshold. Similar to the findings at the 500 hPa level, PPS5 and PPS6 were excluded from this analysis because their factor loading values fell below 0.6, failing to meet the criterion for statistical and physical significance.

Table I also shows that a smaller number of PPSs are required at 500 hPa to explain a larger portion of the variance than at the surface, as a result of the smoother nature of atmospheric fields aloft, which are less influenced by surface-level irregularities.

The 850 hPa level, situated in the lower troposphere, plays a critical role in weather forecasting as it helps delineate the distribution of moist and dry air masses. For the WSM region, the synoptic classification of the specific humidity at this level (q850) revealed five PPSs that together explain 75.8% of the total variance (Table I). Notably, the first four PPSs account for 67.4% of this variance. Similar to the surface (SLP) and upper-level (GH500) analyses, the majority of factor loading values for these PPSs are positive, with many surpassing the 0.6 threshold. However, PPS5 was excluded here due to its factor loading values remaining below 0.6.

The relationships among the three analyzed atmospheric levels (surface, 850 hPa, and 500 hPa) were determined by subjective visual interpretations and by examining the time series of factor loadings for each identified PPS at each level. The strongest correlation among all possible combinations of the three atmospheric levels was identified for:

i. PPS3 at 500 hPa with PPS1 at surface (correlation = 0.71) and with PPS1 at 850 hPa (correlation = 0.33); PPS1 at surface with PPS1 at 850 hPa (correlation = 0.32).

Table I. Percentages of explained variance (P. Var) and cumulative percentages (C.P. Var) explained by the PPSs retained for each meteorological variable (GH500, SLP, and q850).

PPS	GH500		SLP		q850	
	P. Var	C. P. Var	P. Var	C. P. Var	P. Var	C. P. Var
1	32.9	32.9	22.2	22.2	19.7	19.7
2	25.5	58.4	21,3	43.5	17.3	37.0
3	23.0	81.4	12.7	56.2	16.7	53.7
4	8.6	90.0	8.4	64.6	13.7	67.4
5	3.1	93.1	8.1	72.7	8.4	75.8
6	1.3	94.4	4.6	77.3		

PPS: pattern sequence analysis; GH500: geopotential height at 500 hPa; SLP: sea level pressure; q850: specific humidity at 850 hPa.

ii. PPS1 at 500 hPa with PPS2 at surface (correlation = 0.33) and with PPS2 at 850 hPa (correlation = 0.34); PPS2 at surface with PPS2 at 850 hPa (correlation = 0.67).
iii. PPS2 at 500 hPa with PPS3 at surface (correlation = 0.40) and with PPS4 at 850 hPa (correlation = 0.40); PPS3 at surface with PPS4 at 850 hPa (correlation = 0.41).
iv. PPS4 at 500 hPa with PPS4 at surface (correlation = 0.30) and with PPS3 at 850 hPa (correlation = 0.17); PPS4 at surface with PPS3 at 850 hPa (correlation = 0.43)

The statistical significance of the correlation coefficients was assessed using Student's t-test (Kanji, 2006). All coefficients were found to be statistically significant at the 0.05 confidence level.

Four primary synoptic-scale weather patterns associated with HRE in the WSM were identified, as summarized in Table II. These patterns are:

- Cold front with southwesterly wind (CF_s).
- Cyclogenesis (CG).
- Cyclogenesis with blocking (CG_b).
- Cold front with easterly wind (CF_e).

Table II. Relationship of PPSs between the three meteorological variables (GH500, SLP, and q850) for each of the four main synoptic patterns associated with the occurrence of HRE in the WSM (CF_s, CG, CG_b, CF_e).

	GH500	SLP	q850
CF_s	PPS 3	PPS 1	PPS 1
CG	PPS 1	PPS 2	PPS 2
CG_b	PPS 2	PPS 3	PPS 4
CF_e	PPS 4	PPS 4	PPS 3

PPS: pattern sequence analysis; GH500: geopotential height at 500 hPa; SLP: sea level pressure; q850: specific humidity at 850 hPa; CF_s: cold front with southwesterly wind; CG: cyclogenesis; CG_b: cyclogenesis with blocking; CF_e: cold front with easterly wind.

Figure 3 shows the PPSs derived at the 500 hPa level, surface level, and 850 hPa level associated with the CF_s pattern. This synoptic configuration is characteristic of the typical passage of cold fronts across Brazil throughout the year, particularly during the winter and spring seasons (Foss et al., 2017; Escobar et al., 2019a, b; Escobar, 2023).

On Day –2 (Fig. 3a), a low-pressure system is observed over central-northern Argentina, southern Bolivia, and western Paraguay. This system is linked to the NAL or the CHL (Seluchi et al., 2003; Escobar and Seluchi, 2012; Marengo et al., 2012). Simultaneously, a trough is present over southwestern Buenos Aires Province, near 38º S, 62º W, likely associated with an approaching cold front. In the middle troposphere (500 hPa), an anticyclone over the Pacific Ocean extends a ridge into central-northern Argentina, consistent with the thermal low-pressure system observed at the surface. Additionally, a frontal trough is located near 40º S, 65º W, further reinforcing the presence of the aforementioned cold front.

At the 850 hPa level, specific humidity reveals a large moist air mass covering the states of SC, PR, São Paulo (SP), Rio de Janeiro (RJ), southern Minas Gerais (MG), much of the central-west region, and parts of northern and northeastern Brazil. Over PR, the maximum humidity is partly driven by moist northerly winds associated with the low-pressure system described earlier.

By Day –1 (Fig. 3b), the cold front, previously located in Argentina, advances eastward, extending between southern RS and southern Bolivia. At this stage, the WSM of PR experiences moderate northerly winds due to a significant pressure gradient. The specific humidity at 850 hPa remains elevated over PR, while dry air begins to penetrate central Argentina and southern Uruguay, influenced by a post-frontal anticyclone. At 500 hPa, the frontal trough is positioned over Argentina near 57º W, aligning with the surface cold front.

On the day of the HRE (Day 0) in the WSM (Fig. 3c), the frontal trough shifts further eastward, reaching approximately 54º W. As a result, the cold front moves across much of RS and SC, positioning itself between central PR and southwestern Mato Grosso (MT). Over 40º S, 40º W, the low-pressure system associated with the cold front is observed. Under this surface circulation, the WSM of PR experiences moderate southwesterly winds. A similar synoptic pattern was identified by Escobar (2023) during his study on winter-season synoptic classifications in Brazil. The synoptic pattern associated with a cyclogenesis (CG) process is illustrated in Figure 4.

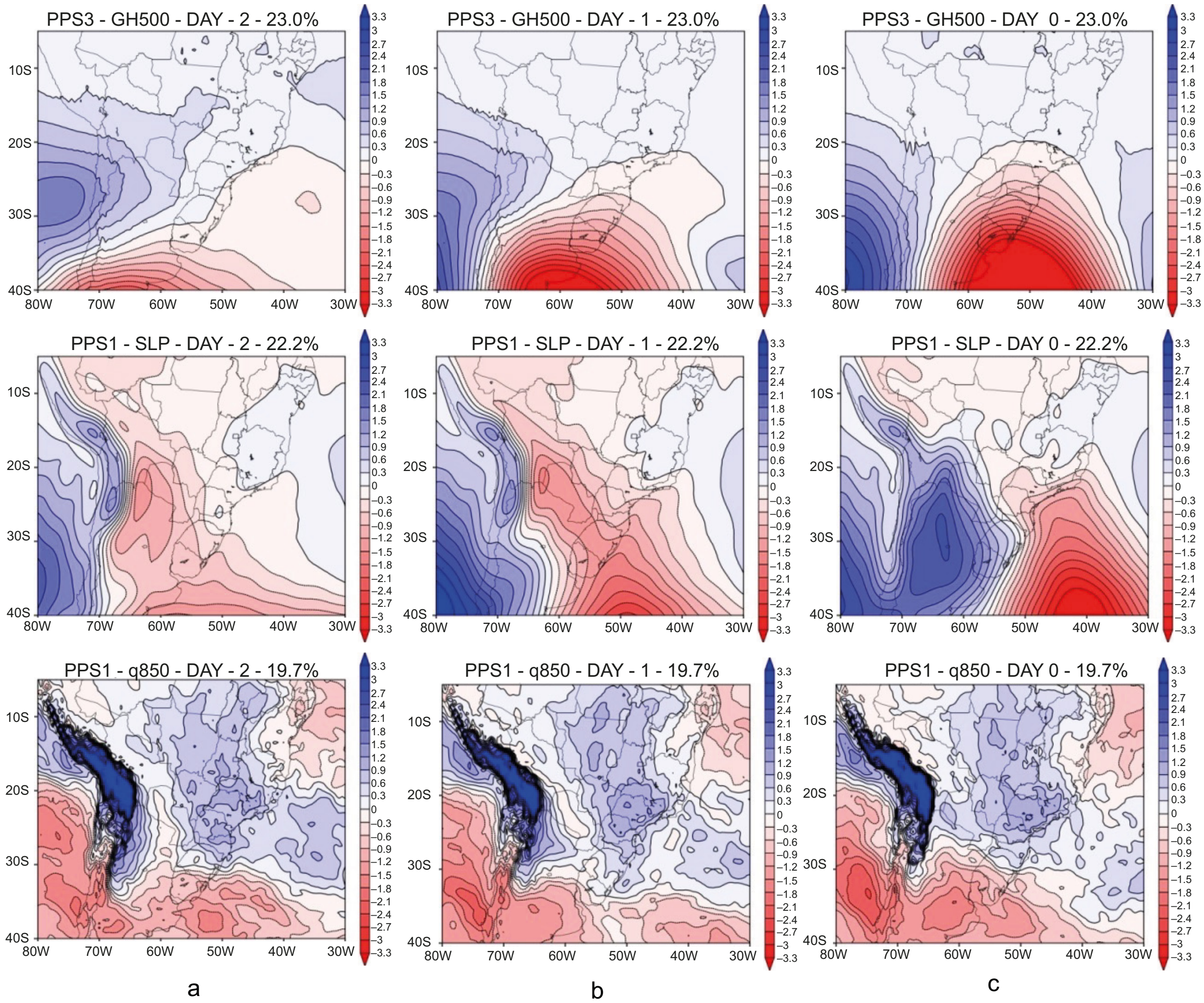

Fig. 3. CF_s pattern (cold front with southwesterly wind). Principal pattern sequence (PPS) obtained at the 500 hPa level, at the surface level, and at the 850 hPa level (top to bottom). From left to right: (a) Day –2; (b) Day –1; (c) Day 0.

Two days before the occurrence of the HRE in the WSM (Day –2 (Fig. 4a), a low-pressure system resulting from the merging of the NAL and the CHL is observed over central-north Argentina, near 30º S, 67º W. In the following days, this low-pressure system moves eastward, forming a cyclone near Uruguay, southeastern RS, and the adjacent Atlantic Ocean by Day 0 (Fig. 4c). Simultaneously, throughout the analyzed period, the South Atlantic Subtropical High (SASH) is observed around 40º S, 43º W on Day –2, which slowly moves eastward in the subsequent days.

During Day –2 and Day –1, significant northerly winds are observed over the WSM of the PR State, promoting the advection of warm and moist air. This contributes to increased instability over the region.

In the middle troposphere, a baroclinic trough is observed moving slowly eastward, promoting the advection of cyclonic vorticity over Paraguay, northeastern Argentina, southern Mato Grosso do Sul (MS) State, and the western south region of Brazil, including the WSM. This favors the formation of the surface cyclone described earlier. Simultaneously, during the analyzed period, a high-pressure system at 500 hPa is located over the Atlantic Ocean near 40º S, also moving slowly eastward. This upper-level high is associated with the SASH, as noted at the surface.

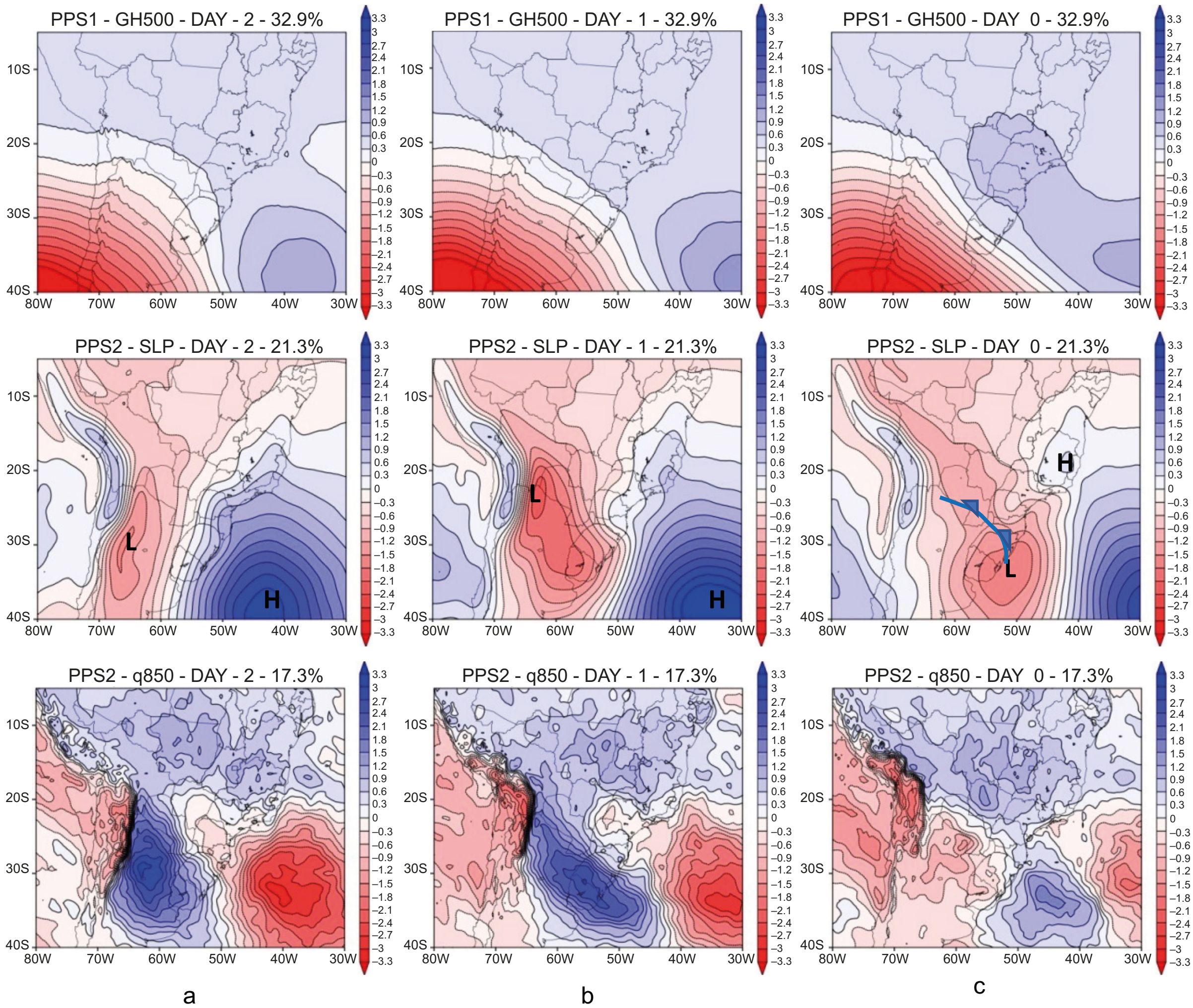

Fig. 4. CG pattern (cyclogenesis). Principal pattern sequence (PPS) obtained at the 500 hPa level, at the surface level, and at the 850 hPa level (top to bottom). From left to right: (a) Day –2; (b) Day –1; (c) Day 0.

On Day –2 (Fig. 4a), the specific humidity at the 850 hPa level shows a significant moisture concentration over central-north Argentina, western Paraguay, and Uruguay. This moisture spreads to the entire RS State, southern and western SC State, and the WSM of the PR State by Day –1 (Fig. 4b). This phenomenon results from the advection of moist air from the Amazon region, driven by the low-pressure system observed at the surface.

By Day 0 (Fig. 4c), the specific humidity begins to decrease, and dry air starts to appear over central-north Argentina, much of Paraguay and Uruguay, and the western south region of Brazil due to the influence of southerly winds. These winds result from the formation of the cold branch of the extratropical cyclone. Thus, the formation of this extratropical cyclone was the main factor related to the HRE that occurred in the WSM of the PR State.

A similar synoptic pattern sequence was identified by Escobar and Barbio (2024) in their analysis of synoptic patterns associated with heavy rainfall events in the metropolitan region of Porto Alegre, Brazil.

The synoptic pattern associated with cyclogenesis and a blocking configuration (CG_b) is shown in Figure 5. On Day –2 (Fig. 5a), a frontal system is observed at the surface near the coast of the PR State, and an inverted trough is positioned over the MS State

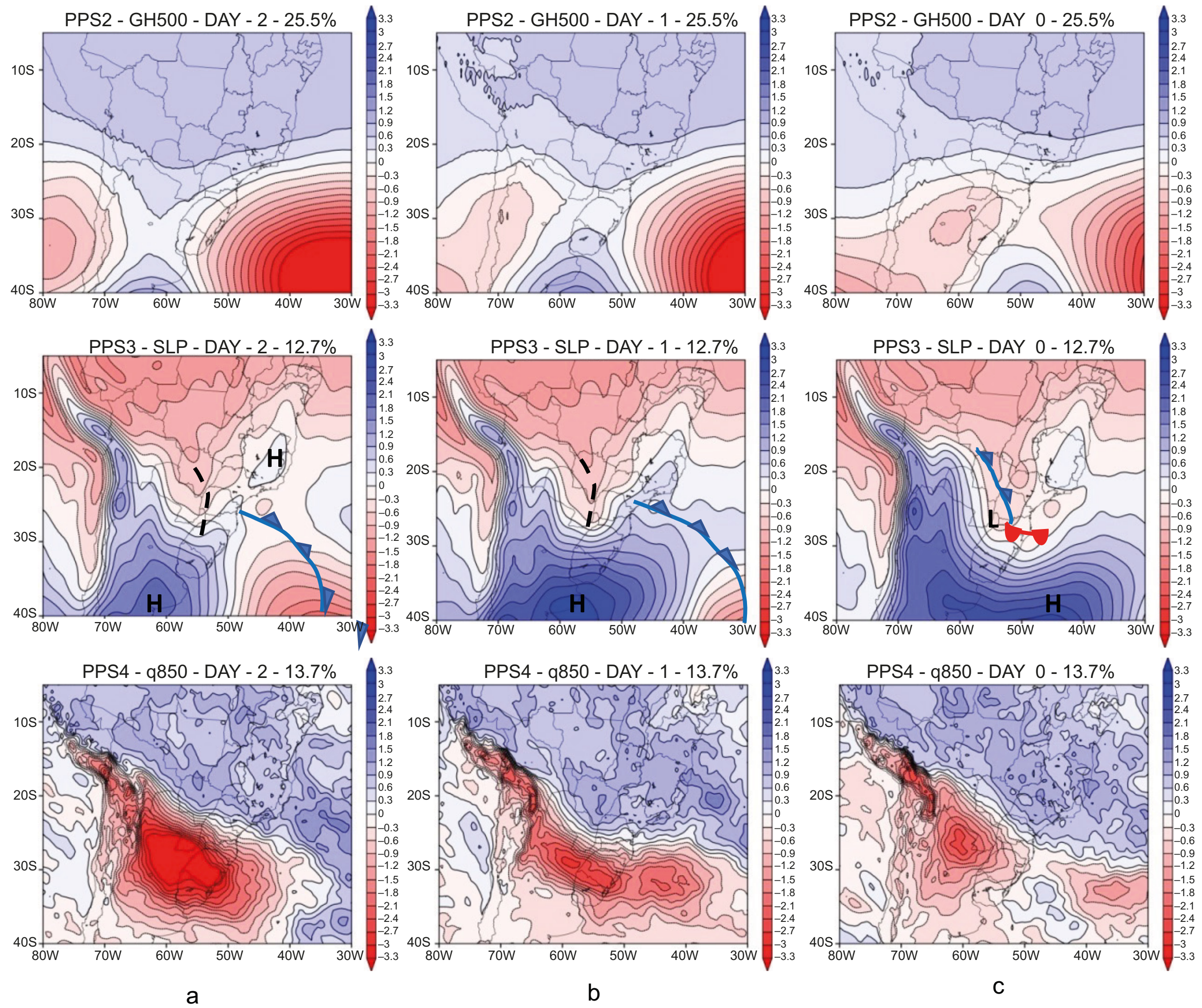

Fig. 5. CG_b pattern (cyclogenesis with blocking). Principal pattern sequence (PPS) obtained at the 500 hPa level, at the surface level, and at the 850 hPa level (top to bottom). From left to right: (a) Day –2; (b) Day –1; (c) Day 0.

and northwestern RS State. By Day –1 (Fig. 5b), the frontal system is located over the southern SP State, with the WSM of the PR State affected by northeasterly winds. These winds are driven by the substantial horizontal pressure gradient created between the anticyclone located around 40º S, 58º W, and the inverted trough positioned over the MS State and northwestern RS State.

On Day 0 (Fig. 5c), the inverted trough intensifies and forms a frontal wave, with the cold branch extending approximately from the western SC State to the southern MT State. To the south of this inverted trough, the anticyclone slowly shifts eastward, positioning itself near 40º S, 50º W by Day 0.

The formation and intensification of this inverted trough are linked to the presence of a cyclonic vortex in the middle troposphere. On Day –2 (Fig. 5a), the low-pressure system at 500 hPa is located over the Pacific Ocean, near the coast of Chile, at around 35º S, 80º W. By Day –1, the cyclonic vortex begins to cross the Andes, and by Day 0, it is positioned over northeastern Argentina, near 32º S, 63º W. The trough associated with this vortex extends in a southwest-northeast orientation, affecting the western portion of the south region of Brazil, including the WSM of the PR State.

Simultaneously, an upper-level high-pressure system is present near 40º S, 63º W on Day –2. It slowly moves eastward over the following days, positioning near 40º S, 49º W by Day 0.

Both the high- and low-pressure systems at altitude are nearly in phase with the surface systems, establishing a barotropic pattern similar to that of blocking configurations (Sinclair 1996).

The specific humidity at 850 hPa shows a moist area extending from the Atlantic Ocean into the interior of the continent, affecting a large part of the southeast and central-west regions, as well as portions of the north and northeast of the country. This pattern is associated with the presence of a stationary front located over the Atlantic Ocean and its alignment with the moisture advection from the continent.

Due to the presence of the stationary front and the formation of a frontal wave between the northern RS State and southwestern PR State, a dry air mass remains concentrated over Uruguay, the entire RS State, much of SC State, the WSM of PR State, central-north and northeastern Argentina, southern Paraguay, and southern Bolivia during Day –2 (Fig. 5a). On Day –1 (Fig. 5b), a tongue of moist air mass can be seen descending from MT toward the states of PR and SC, due to the intensification of the inverted trough observed at the surface. By Day 0 (Fig. 5c), moisture begins to decrease over the WSM due to the southerly winds generated by the cyclogenesis process. With such a weather pattern, the WSM of PR increases its specific humidity and mass convergence, which favors the intensification of rainfall in the study region.

This synoptic pattern is similar to the one identified by Escobar et al. (2019b) in their study of the synoptic climatology associated with “friagens” episodes in the city of Cuiabá, MT, and by Müller et al. (2003) when they studied the surface circulation associated with frost in the wet pampas of Argentina.

Finally, the last main synoptic pattern associated with the occurrence of HRE in the WSM is also related to the passage of a cold front (CF_e), but with a different position compared to the CF_s pattern. Figure 6 shows the PPSs obtained at 500 hPa, the surface level, and 850 hPa for this pattern.

On Day –2 (Fig. 6a), the cold front appears approximately over southern RS, connected to the CHL located over northern Argentina, western Paraguay, and southern Bolivia. At the same time, an anticyclone system is observed over the MG State, approximately at 19º S, 43º W. This anticyclone is an extension of the SASH, positioned approximately at 35º S, 30º W, likely related to an old migratory anticyclone. Both of these systems (the CHL and the anticyclone) produce a significant horizontal pressure gradient, resulting in moderate northwesterly winds over the WSM. Consequently, this region is dominated by a moist and warm air mass from the Amazon region, leading to high values of specific humidity at the 850 hPa level.

On Day –1 (Fig. 6b), the frontal system arrives in the eastern part of the SC State. At the same time, the CHL is observed over northern Argentina, while the post-frontal anticyclone begins to extend over central Argentina, Uruguay, and southern RS. Consequently, the dry air mass advances into northeastern Argentina, Uruguay, and southern RS, as observed at the 850 hPa level.

On Day 0 (Fig. 6c), the cold front slowly moves eastward and positions itself in the southern part of the SP State. The center of the post-frontal anticyclone moves eastward and positions itself near 35 ºS, 50 ºW. Thus, due to the zonal movement of the migratory anticyclone, the WSM of PR State experiences no change in wind direction and continues to be influenced by northerly winds associated with a trough located between northern Argentina and southern Bolivia. In agreement with this weather pattern, the highest specific humidity values at low levels are concentrated over SC, a significant portion of the PR State, northeastern Paraguay, southern and western MS, eastern and northeastern Bolivia, and the southern part of the north region of Brazil. The 500 hPa level shows a typical baroclinic trough advancing eastward, with its axis extending in a northwesterly/southeasterly orientation.

On Day –2 (Fig. 6a), this mid-level low-pressure system is located between northeastern Argentina and the Atlantic Ocean, and by Day 0 (Fig. 6c), it is positioned over eastern SC. Ahead of this trough, there is a high-pressure system with wide coverage, extending over a significant portion of the Southeast and Central-West regions of Brazil and the adjacent Atlantic Ocean. This high-pressure system is reflected at the surface by the presence of the SASH, which also extends into the continent through a relative high-pressure area over southeastern Brazil.

Additionally, there is another high-pressure system at 500 hPa that enters the continent during the

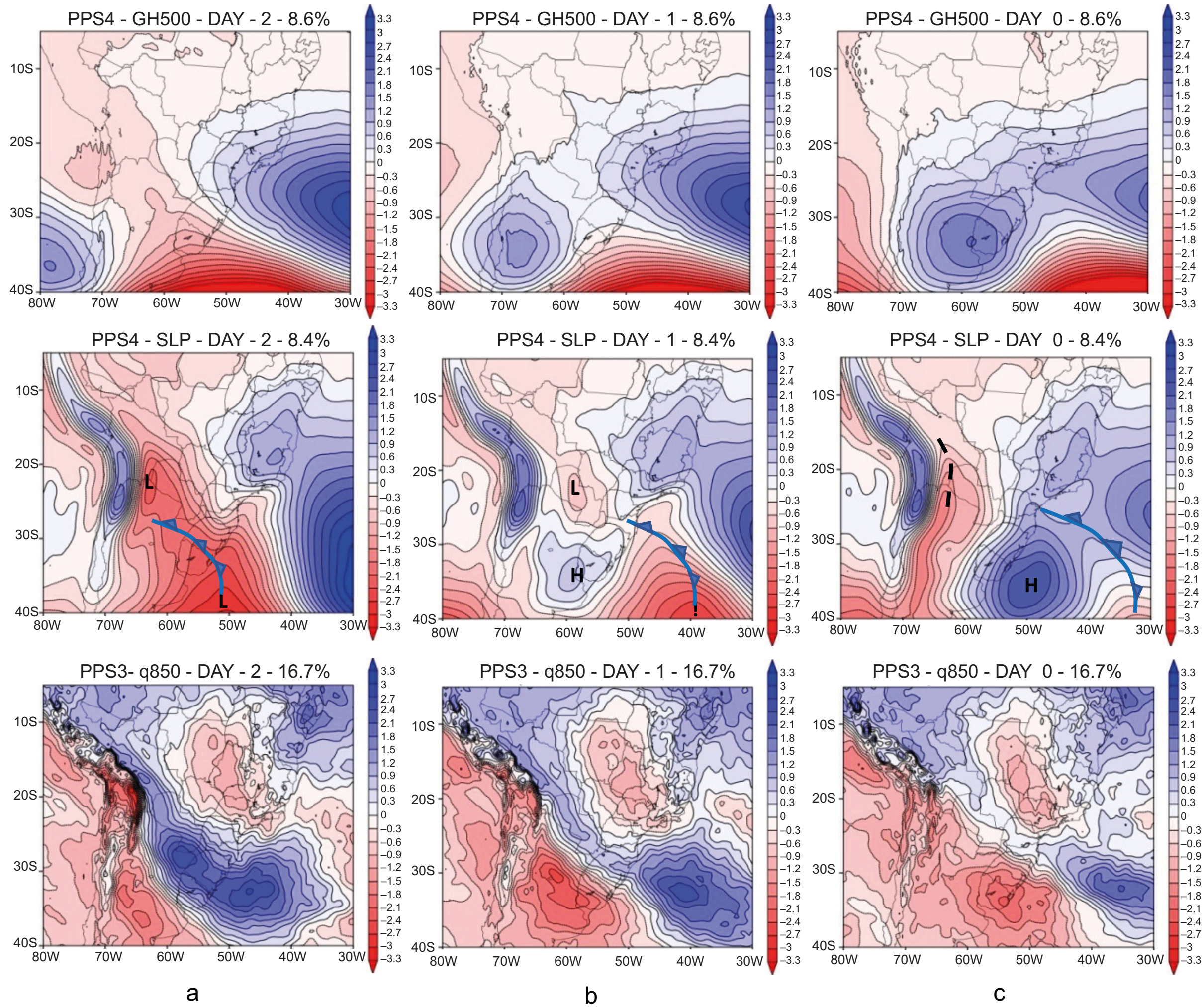

Fig. 6. CF_e pattern (cold front with easterly wind). Principal pattern sequence (PPS) obtained at the 500 hPa level, at the surface level, and at the 850 hPa level (top to bottom). From left to right: (a) Day –2; (b) Day –1; (c) Day 0.

analyzed period. On Day –2, this anticyclone is located over central Chile and the adjacent Pacific Ocean, and by Day 0, it is observed centered between Argentina and Uruguay, around 33ºS, 58ºW. This high-pressure system is related to the migratory post-frontal anticyclone mentioned at sea level pressure.

Under this weather pattern, the WSM of PR exhibits northerly winds throughout the entire analyzed period, which favors the concentration of high specific humidity values in the study region. This was likely the primary factor contributing to the occurrence of HRE. This synoptic pattern sequence closely resembles that identified by Escobar et al. (2024) during the heavy rainfall event in RS from late April to early May 2024.

The four synoptic types related to HRE in the WSM of PR exhibit distinct dynamical and thermodynamical characteristics. The CF_s pattern reflects a classic cold-frontal passage, with a progressive eastward-moving baroclinic system, moderate pre-frontal northerly flow, and sustained moisture advection leading to widespread rainfall. In contrast, the CG type is driven by extratropical cyclogenesis off the southern coast, featuring strong low-level moisture transport from the Amazon, significant baroclinicity, and cyclonic development that maximizes rainfall just before frontal passage. The CG_b configuration combines cyclogenesis with a blocking-like pattern: an upper-level trough crossing the Andes interacts with a surface inverted trough and a persistent anticyclone, resulting in prolonged moisture convergence and enhanced rainfall. Finally, the CF_e type involves a more zonally displaced cold front, where a continental high over southeastern Brazil maintains persistent northerly winds over the WSM throughout the event, preventing post-frontal drying and enabling continuous moisture supply and rainfall intensification. While all types rely on low-level moisture advection and baroclinic forcing, they differ in frontal mobility and upper-level support-key factors determining HRE in the study region.

The distribution of variance explained by the four synoptic patterns (CF_s, CG, CG_b, CF_e) (at surface) across different seasons is presented in Table III.

Table III. Percentages of total explained variance and variance accumulated by the four main synoptic patterns (CF_s, CG, CG_b, CF_e) (at surface) during the different seasons of the year, associated with HRE in the WSM.

Season	CF_s	CG	CG_b	CF_e
Summer	5.7	3.9	1.0	1.9
Autumn	6.5	5.7	4.7	1.5
Winter	3.5	2.0	3.7	2.7
Spring	6.5	9.7	3.3	2.3
Total	22.2	21.3	12.7	8.4

CF_s: cold front with southwesterly wind; CG: cyclogenesis; CG_b: cyclogenesis with blocking; CF_e: cold front with easterly wind; HRE: heavy rainfall events; WSM: western and southwestern mesoregions of the State of Paraná.

The CF_s pattern shows a consistent contribution throughout the year, primarily during autumn and spring, where it reaches its highest values (6.5%).

On the other hand, the CG pattern also exhibits the highest percentages of explained variance during autumn (5.7%) and spring (9.7%). However, during the rest of the year (summer and winter), it shows lower percentages of explained variance (3.9% and 2.0%, respectively).

The highest explained variance percentages exhibited by these synoptic patterns (CF_s and CG) are consistent. This is because, during these seasons, temperature and humidity become more significant, and baroclinic systems remain relevant in the southern region of Brazil. As a result, the WSM of PR State experiences more intense and severe rainfall compared to other times of the year.

The CB_b pattern displays the lowest percentages of explained variance during summer (1.0%) and the highest values during winter (3.7%) in comparison to the other patterns. This pattern shows its highest values during autumn (4.7%) and is typically associated with cold surges in South America, as shown in Figure 5.

Finally, the CF_e pattern has the lowest explained variance in autumn (1.5%) and shows its major contributions in winter (2.3%).

3.2 Composites for the thermal infrared image associated with HRE in the WSM

Following the synoptic classification of atmospheric patterns associated with HRE in the study region, we generated composite fields of thermal infrared imagery and mean sea level pressure (SLP) for the four predominant synoptic patterns (CF_s, CG, CG_b, CF_e) identified in section 3.1. These composites were calculated using cases that exhibited a high correlation with each PPS at the surface, selecting those with loadings ≥ 0.6 (Richman and Gong, 1999). This selection yielded 45 cases for the CF_s pattern, 36 for the CG pattern, 20 for the CG_b pattern, and 9 for the CF_e pattern. Table IV presents the dates associated with each of the four main synoptic patterns linked to HRE occurrences in the WSM of PR.

The resulting composites for thermal infrared imagery and SLP, spanning from Day –2 to Day 0 of the HRE in the WSM of PR, are presented in Figure 7.

The CF_s pattern on Day –2 shows the presence of a cold front in Argentina, near the latitude of the province of Buenos Aires. Associated with this frontal system is a band of cloudiness with brightness temperatures around 260 K, indicating weak convective activity or stratiform clouds. Over Uruguay, northeastern Argentina, and much of southern Brazil, there is low cloudiness linked to the presence of stratiform clouds, with brightness temperatures around 270 K.

By Day –1, this pattern reveals the development of deep clouds over the states of RS, SC, and the southern and southwestern parts of PR. The maximum intensity of these clouds is centered around

Table IV. Dates (month/date/year) of HRE related to the four main synoptic patterns (CF_s, CG, CG_b, CF_e).

CF_s	CG	CG_b	CF_e
12/30/2000	10/01/2001	04/04/2003	09/13/2000
12/22/2001	10/08/2001	05/042004	10/14/2000
09/01/2002	09/20/2002	05/13/2004	06/07/2001
11/04/2002	04/19/2003	09/13/2004	05/16/2002
12/24/2002	10/09/2003	06/16/2005	06/07/2014
12/12/2003	10/26/2003	10/17/2005	07/02/2015
01/25/2005	11/17/2003	05/18/2010	07/11/2015
05/21/2005	10/17/2004	08/01/2011	12/20/2015
10/05/2005	09/20/2006	04/29/2012	09/20/2018
10/29/2005	10/12/2009	06/25/2013	
04/15/2006	12/12/2009	06/28/2014	
08/16/2006	04/26/2010	10/10/2015	
12/21/2006	12/03/2010	05/09/2016	
04/25/2007	11/22/2011	05/21/2016	
04/26/2007	03/05/2014	04/16/2017	
05/08/2007	03/31/2014	09/02/2018	
12/06/2007	05/01/2014	01/20/2021	
04/14/2008	09/07/2014	06/02/2022	
05/14/2009	11/28/2015	06/03/2022	
06/24/2009	10/13/2016	08/07/2022	
07/11/2009	10/26/2016		
09/23/2009	11/02/2016		
01/13/2010	12/03/2016		
03/15/2010	04/26/2017		
04/23/2010	15/19/2017		
12/05/2010	10/26/2017		
12/13/2010	11/04/2017		
10/30/2011	11/27/2019		
03/13/2013	12/16/2019		
05/16/2013	03/19/2020		
07/24/2014	12/03/2020		
11/20/2015	01/17/2021		
12/10/2015	10/14/2021		
08/20/2017	10/15/2021		
10/22/2017	03/25/2022		
05/19/2018	04/12/2022		
02/12/2019			
02/26/2019			
04/05/2019			
12/05/2019			
02/26/2020			
08/19/2020			
10/04/2021			
10/24/2021			
08/18/2022			

HRE: heavy rainfall events; CF_s: cold front with southwesterly wind; CG: cyclogenesis; CG_b: cyclogenesis with blocking; CF_e: cold front with easterly wind.

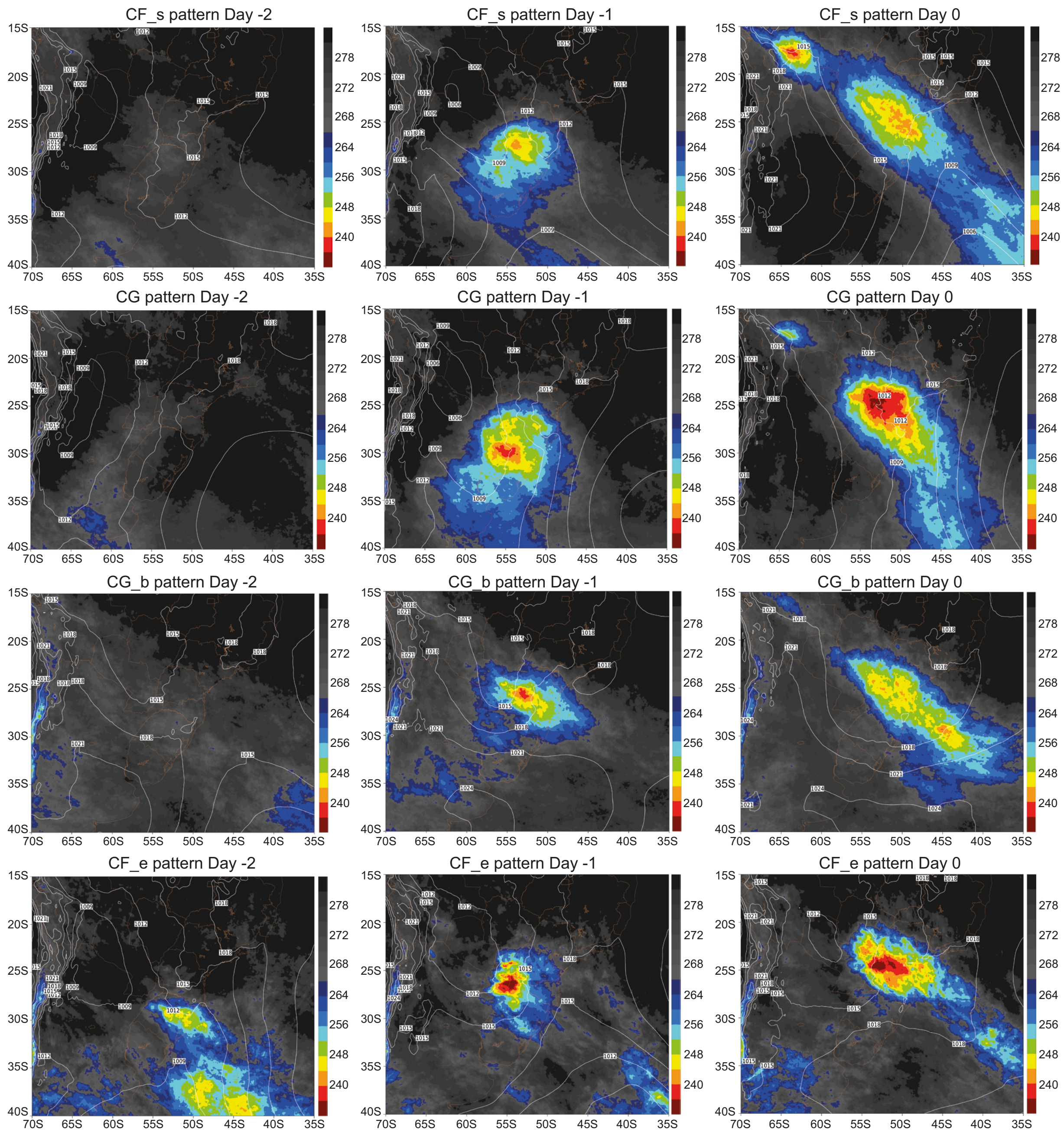

Fig. 7. Composites of GOES-East thermal infrared image (in K, shaded) and SLP (each 3 hPa in lines) associated with HRE in the WSM. From top to bottom: CF_s pattern, CG pattern, CG_b pattern, and CF_e pattern. From left to right: Day –2, Day –1, Day 0. (GOES: Geostationary Operational Environmental Satellite; SLP: sea level pressure; HRE: heavy rainfall events; WSM: western and southwestern mesoregions of the State of Paraná.)

northwestern RS and western SC, with brightness temperatures around 240 K.

This cloud formation was primarily associated with prefrontal activity, as the cold front on this day was positioned near northern Uruguay, northeastern Argentina, and the southern RS State, as illustrated in Figure 7.

On Day 0, a cloud band extends from southern Bolivia to the Atlantic Ocean, aligned with the frontal system. Two convective systems are observed: one over Bolivia and the other over PR, with brightness temperatures around 240 K and 244 K, respectively. Under this weather pattern, the WSM is influenced by convective activity on Day –1 and stratiform clouds on Day 0.

In the CG pattern, during Day –2, the presence of a continental low-pressure system resulting from the merging of the NAL and the CHL can be observed in northern Argentina, southern Bolivia, and western Paraguay. The northerly winds generated by this system facilitate the advection of warm and moist air masses from the Amazon Basin. This contributes to the formation of stratiform clouds (270 K) over northeastern Argentina and western southern Brazil, including the WSM.

To the south of this area of low pressure, there are shallow convective cells (260 K), likely related to the presence of a trough located around 40º S, 65º W.

On Day –1, the low-pressure system intensifies and moves toward the southeast, contributing to the formation of a large area with deep clouds centered over the RS State, characterized by a brightness temperature below 244 K. On several occasions, these deep clouds are associated with the formation of MCS (Salio et al., 2007), driven by the inflow of warm and moist air generated by the low-pressure system.

One day later (Day 0), the convective system increased in size and strength, moving toward the northeast and reaching a brightness temperature below 235 K. This convective system was concentrated over a large portion of the PR State, including the WSM. At the same time, the extratropical cyclone formed around 37º S, 50º W, with its associated cold front extending toward eastern Paraguay. With this synoptic pattern, the HRE occurs in the WSM during extratropical cyclone formation, approximately between Day –1 and Day 0.

The CG_b pattern also shows the presence of deep clouds for one day before the occurrence of HRE in the WSM (Day –1). On this day, there is a large convective system covering a great part of the SC State and the southwestern part of PR, with its maximum intensity centered around the WSM, with a brightness temperature around 240 K. This convective system is formed to the north of the stationary front, in the warm, moistly and unstable air, as described in Figure 5.

On Day 0, the extratropical cyclone begins to form around northeastern RS and eastern SC, with its associated cold front extending into Paraguay. In this situation, a band of cloudiness covers the states of SC and PR, with brightness temperatures ranging between 240 and 248 K. The spatial distribution of the clouds associated with this weather pattern is similar to that observed in the CF pattern.

Finally, the CF_e pattern is also associated with the passage of a cold front; however, it does not pass over the WSM of PR State due to its zonal translation.

On Day –2, the cold front is observed between southern RS and northeastern Argentina, where a low-pressure system is located. Ahead of this frontal system, particularly over northeastern RS, deep clouds with brightness temperatures around 248 K are present. By Day –1, the cold front has moved over the Atlantic Ocean, close to the southern coast of the SC State. Simultaneously, the low-pressure system associated with the merging of the NAL and the CHL intensifies and shifts southeastward, affecting northwestern RS, western SC, the WSM of PR, and southeastern Paraguay. Over this region, deep convective clouds with brightness temperatures around 234 K are observed.

On Day 0, the cold front is located over the Atlantic Ocean at the latitude of RS, far from the continent. The convective system moves slowly northeastward, covering a large portion of the PR State. The maximum intensity of this system occurs over western and northern PR, with brightness temperatures around 234 K. This meteorological pattern also features a band of cloudiness extending into the ocean, aligned with the surface oceanic frontal band.

4. Conclusions

This study developed a synoptic classification to identify the main patterns associated with HRE in the WSM of PR State, based on 178 events (2000-2022) exceeding the daily precipitation threshold of 32.8 mm. HREs peaked in May and October—periods characterized by enhanced moisture availability and baroclinic activity—and were least frequent in summer (limited by weak baroclinicity) and winter (constrained by low atmospheric moisture).

Four dominant synoptic types emerged, consistent with weather regimes recognized by experienced forecasters: two linked to cold-front passages (CF_s and CF_e), differing in anticyclone trajectory and persistence of low-level moisture; and two associated with cyclogenesis (CG and CG_b). The CF_e and CG patterns exhibited the strongest convective activity (infrared brightness temperatures < 240 K), driven by the merger of the NAL and CHL, which sustained moisture advection from the Amazon Basin into the WSM. In contrast, the CG_b type involved a blocking configuration that promoted frontal wave development and mass convergence despite relatively modest low-level humidity.

The main contribution of this paper, compared to previous studies, is the objective identification of synoptic pattern sequences associated with HRE in the WSM. This approach enables systematic analysis of the development, evolution, and vertical structure of synoptic systems across the main tropospheric levels. In operational forecasting centers, meteorologists are familiar with these situations, but their recognition is often subjective and experience-dependent. An objective, reproducible classification reduces subjectivity and supports faster, more effective forecasting, a critical advantage in operational environments.

Acknowledgments

The authors thank the National Institute for Space Research (INPE) of Brazil for the satellite images and the National Center for Environmental Prediction (NCEP) for the reanalysis data. We also express our gratitude to the Brazilian Research Council (CNPq) for financial support ("Edital universal" grant number 402554/2021-3).

References

Andrade KM. 2005. Climatologia e comportamento dos sistemas frontais sobre a América do Sul. M.Sc. thesis. Instituto Nacional de Pesquisas Espaciais (INPE).

Balicki M, Andrade AR, Hornes KL. 2020. Gênese e impacto de tempestades severas no estado do Paraná (Brasil). Revista Brasileira de Climatologia 26: 479-498. https://doi.org/10.5380/abclima.v26i0.71335

Bugoni Riquetti N, Rodrigues Dorneles V, Becker Nunes A. 2018. Estudo de caso de precipitação intensa sobre Foz do Iguaçu-PR em setembro de 2015. Revista Brasileira de Climatologia 22: 589-606. https://doi.org/10.5380/abclima.v22i0.58304

Cavalcanti IFA, Kousky VE. 2009. Frentes frias sobre o Brasil. In: Tempo e clima no Brasil (Cavalcanti IFA, Ferreira NJ, Silva MGAJ, Dias MAFS, Eds.). Oficina de Textos, São Paulo.

Carvalho LMV, Jones C, Liebmann B. 2002. Extreme precipitation events in southeastern South America and large-scale convective patterns in the South Atlantic Convergence Zone. Journal of Climate 15: 2377-2394. https://doi.org/10.1175/1520-0442(2002)015%3C2377:EPEISS%3E2.0.CO;2

Castañeda ME, Ulke AG. 2015. Analysis of atmospheric conditions associated to CHACO events of the low level jet east of the Andes and their implications for regional transport. International Journal of Climatology 35: 4126-4138. https://doi.org/10.1002/joc.4272

Cattell R. 1978. The scientific use of factor analysis in behavioral and life sciences. Plenum Press, New York and London, 618 pp.

Compagnucci R, Salles MA. 1997. Surface pressure patterns during the year over southern South America. International Journal of Climatology 17: 635-653. https://doi.org/10.1002/(SICI)1097-0088(199705)17:6<635::AID-JOC81>3.0.CO;2-B

Compagnucci R, Araneo D, Canziani P. 2001. Principal sequence pattern analysis: A new approach to classifying the evolution of atmospheric systems. International Journal of Climatology 21: 197-217. https://doi.org/10.1002/joc.601

Da Silva ED, Reboita MS. 2014. Estudo da precipitação no Estado de Minas Gerais – MG. Revista Brasileira de Climatologia 13: 120-136. https://doi.org/10.5380/abclima.v13i0.33345

Dereczynski CP, de Oliveira JS, Machado CO. 2009. Climatologia da precipitação no município do Rio de Janeiro. Revista Brasileira De Meteorologia 24: 24-38. https://doi.org/10.1590/S0102-77862009000100003

Dos Santos DF, Reboita MS. 2018. Jatos de baixos níveis a leste dos Andes: comparação entre duas reanálises. Revista Brasileira de Climatologia 22: 423-445. https://doi.org/10.5380/abclima.v22i0.47595

Dyer RA. 1994. A review of tornado activity in Brazil. In: Proceedings of the International Society for Photogrammetry and Remote Sensing 30: 203-213. INPE, São José dos Campos, Brazil.

Escobar GCJ, Compagnucci RH, Bischoff SA. 2004. Sequence patterns of 1000 hPa and 500 hPa geopotential height fields associated with cold surges in Buenos Aires. Atmósfera 12: 69-89.

Escobar GCJ, Seluchi ME. 2012. Classificação sinótica dos campos de pressão atmosférica na América do Sul e sua relação com as Baixas do Chaco e do Noroeste Argentino. Revista Brasileira de Meteorologia 27: 365-375. https://doi.org/10.1590/S0102-77862012000300011

Escobar GCJ, Seluchi ME, Andrade K. 2016. Classificação sinótica de frentes frias associadas a chuvas extremas no leste de Santa Catarina (SC). Revista Brasileira de Meteorologia 31: 649-661. https://doi.org/10.1590/0102-7786312314b20150156

Escobar GCJ. 2019. Classificação sinótica durante a estação chuvosa do Brasil. Anuário do Instituto de Geociências 42: 421-436. https://doi.org/10.11137/2019_2_421_436

Escobar GCJ, Reboita MS, Souza A. 2019a. Climatology of surface baroclinic zones in the coast of Brazil. Atmósfera 32: 129-141. https://doi.org/10.20937/ATM.2019.32.02.04

Escobar GCJ, Vaz JCM, Reboita MS. 2019b. Surface atmospheric circulation associated with "Friagens" in Central West Brazil. Anuário do Instituto de Geociências 42: 241-254. https://doi.org/10.11137/2019_1_241_254

Escobar GCJ, Reboita MS. 2022. Relationship between daily atmospheric circulation patterns and South Atlantic Convergence Zone (SACZ) events. Atmósfera 35: 1-25. https://doi.org/10.20937/ATM.52936

Escobar GCJ. 2023. Classification of wintertime daily atmospheric circulation patterns over Brazil. Atmósfera 37: 345-363. https://doi.org/10.20937/ATM.53176

Escobar GCJ, Pinto da Rocha F, Arsego, DA, Guedes do Nacimento M, Carvalho da Costa I. 2024. Evento extremo no Rio Grande do Sul entre final de abril e início de maio de 2024. Instituto Nacional de Pesquisas Espaciais. https://www.gov.br/inpe/pt-br/assuntos/ultimas-noticias/relatorio-do-inpe-explica-evento-meteorologico-que-causou-a-tragedia-no-rs/chuvas-rio-grande-do-sul.pdf (accessed on July 5, 2024).

Escobar GCJ, Barbio Rosa M. 2024. Synoptic patterns associated with heavy rainfall events in the metropolitan region of Porto Alegre, Brazil. Meteorology and Atmospheric Physics 136: 40. https://doi.org/10.1007/s00703-024-01041-z

Ferreira V, Goede V, de Lima Nascimento E. 2022. An environmental and polarimetric study of the 19 November 2015 supercell and multiple-vortex tornado in Marechal Cândido Rondon, southern Brazil. Meteorology and Atmospheric Physics 82: 134. https://doi.org/10.1007/s00703-022-00922-5

Foss M, Chou SC, Seluchi ME. 2017. Interaction of cold fronts with the Brazilian plateau: A climatological analysis. International Journal of Climatology 37: 3644-3659. https://doi.org/10.1002/joc.4945

Gozzo LF, de Rocha RP, Reboita MS, Sugahara S. 2014. Subtropical cyclones over the southwestern South Atlantic: Climatological aspects and case study. Journal of Climate 27: 8543-8562. https://doi.org/10.1175/JCLI-D-14-00149.1

Green PE, Carroll, JD. 1978. Analyzing multivariate data. The Dryden Press, Hinsdale.

Harman H. 1976. Modern factor analysis. The University of Chicago Press, Chicago and London.

Hersbach H, Bell B, Berrisford P, Hirahara S, Horányi A, Muñoz-Sabater J, Nicolas J, Peubey C, Radu R, Schepers D, Simmons A, Soci C, Abdalla S, Abellan X, Balsamo G, Bechtold P, Biavati G, Bidlot J, Bonavita M, De Chiara G, Dahlgren P, Dee D, Diamantakis M, Dragani R, Flemming J, Forbes R, Fuentes M, Geer A, Haimberger L, Healy S, Hogan RJ, Hólm E, Janisková M, Keeley S, Laloyaux P, Lopez P, Lupu C, Radnoti G, de Rosnay P, Rozum I, Vamborg F, Villaume S, Thépaut J-N. 2020. The ERA5 global reanalysis. Quarterly Journal of the Royal Meteorological Society 146: 1999-2049. https://doi.org/10.1002/qj.3803

Hoskins BJ, Hodges KI. 2005. New perspectives on the Southern Hemisphere storm tracks. Journal of Climate 18: 4108-4129. https://doi.org/10.1175/JCLI3570.1

Huth R, Beck C, Philipp A, Demuzere M, Ustrnul Z, Cahynová M, Kyselý J, Tveito OT. 2008. Classifications of atmospheric circulation patterns. Recent advances and applications. Trends and Directions in Climate Research: Annals of the New York Academy of Sciences 1146:105-152. https://doi.org/10.1196/annals.1446.019

Kanji GK. 2006. 100 Statistical tests. Sage Publications, London, California, and New Delhi.

Knapp KR, Ansari S, Bain CL, Bourassa, MA, Dickinson MJ, Funk C, Helms CN, Hennon CC, Holmes CD, Huffman GJ, Kossin JP, Lee H-T, Loew A, Magnusdottir G. 2011. Globally gridded satellite observations for climate studies. Bulletin of the American Meteorological Society 92: 893-907. https://doi.org/10.1175/2011BAMS3039.1

Kutner MH, Nachtsheim CJ, Neter J, Li W. 2005. Applied linear statistical models. McGraw-Hill/Irwin, New York.

Lackmann G. 2015. Midlatitude synoptic meteorology: Dynamics, analysis, and forecasting. American Meteorological Society, Boston.

Liebmann B, Jones C, De Carvalho LMV. 2001. Interannual variability of daily extreme precipitation events in the State of São Paulo, Brazil. Journal of Climate 14: 208-218. https://doi.org/10.1175/1520-0442(2001)014%3C0208:IVODEP%3E2.0.CO;2

Maddox RA. 1980. Mesoscale convective complexes. Bulletin of the American Meteorological Society 61: 1374-1387. https://doi.org/10.1175/1520-0477(1980)061%3C1374:MCC%3E2.0.CO;2

Marengo JA, Soares WR, Saulo C, Nicolini M. 2004. Climatology of the low-level jet east of the Andes as derived from the NCEP NCAR reanalyses: Characteristics and temporal variability. Journal of Climate 17: 2261-2280. https://doi.org/10.1175/1520-0442(2004)017%3C2261:COTLJE%3E2.0.CO;2

Marengo JA, Liebmann B, Grimm AM, Misra V, Silva Dias PL, Calvalcanti IFA, Carvalho LMV, Berbery EH, Ambrizzi T, Vera CS, Saulo AC, Nogues-Paegle J, Zipser E, Seth A, Alves LM. 2012. Recent developments on the South American monsoon system. International Journal of Climatology 32: 1-21. https://doi.org/10.1002/joc.2254

Montini TL, Jones C, Carvalho LMV. 2019. The South American low-level jet: A new climatology, variability, and changes. Journal of Geophysical Research, Atmospheres 124: 1200-1218. https://doi.org/10.1029/2018JD029634

Moraes FDS, Aquino FE, Mote TL, Durkee JD, Mattingly KS. 2020. Atmospheric characteristics favorable for the development of mesoscale convective complexes in southern Brazil. Climate Research 80: 43-58. https://doi.org/10.3354/cr01595

Müller GV, Compagnucci R, Nuñez MN, Salles A. 2003. Surface circulation associated with frost in the wet pampas. International Journal of Climatology 23: 943-961. https://doi.org/10.1002/joc.907

Rasmussen KL, Chaplin MM, Zuluaga MD, Houze Jr RA. 2016. Contribution of heavy convective storms to rainfall in South America. Journal of Hydrometeorology 17: 353-367, https://doi.org/10.1175/JHM-D-15-0067.1

Reboita MS, Gan MA, da Rocha RP, Ambrizzi T. 2010a. Regimes de precipitação na América do Sul: uma revisão bibliográfica. Revista Brasileira de Meteorologia 25: 185-204. https://doi.org/10.1590/S0102-77862010000200004

Reboita MS, da Rocha RP, Ambrizzi T, Sugahara S. 2010b. South Atlantic Ocean cyclogenesis climatology simulated by regional climate model (RegCM3). Climate Dynamics 35: 1331-1347. https://doi.org/10.1007/s00382-009-0668-7

Richman MB. 1986. Rotation of principal components. Journal of Climatology 6: 293-335. https://doi.org/10.1002/joc.3370060305

Richman M, Angel J, Gong X. 1992. Determination of dimensionality in Eigenanalysis. In: Proceedings of the 5th International meeting on statistical climatology, Toronto, Canada.

Richman MB, Gong X. 1999. Relationships between the definition of the hyperplane width to the fidelity of principal component loadings patterns. Journal of Climate 12: 1557-1576. https://doi.org/10.1175/1520-0442(1999)012%3C1557:RBTDOT%3E2.0.CO;2

Rozante JR, Vila DA, Barboza Chiquetto J, Fernandes AA, Souza Alvim D. 2018. Evaluation of TRMM/GPM blended daily products over Brazil. Remote Sensing 10: 882. https://doi.org/10.3390/rs10060882

Rozante JR, Gutierrez ER, Fernandes A de A, Vila DA. 2020. Performance of precipitation products obtained from combinations of satellite and surface observations. International Journal of Remote Sensing 41: 7585-7604. https://doi.org/10.1080/01431161.2020.1763504

Saha S, Moorthi S, Pan H-L, Wu X, Wang J, Nadiga S, Tripp P, Kistler R, Woollen J, Behringer D, Liu H, Stokes D, Grumbine R, Gayno G, Wang J, Hou Y-T, Chuang H-y, Juang H-MH, Sela J, Iredell M, Treadon R, Kleist D, Van Delst P, Keyser D, Derber J, Ek M, Meng J, Wei H, Yang R, Lord S, van den Dool H, Kumar A, Wang W, Long C, Chelliah M, Xue Y, Huang B, Schemm J-K, Ebisuzaki W, Lin R, Xie P, Chen M, Zhou S, Higgins W, Zou C-Z, Liu Q, Chen Y, Han Y, Cucurull L, Reynolds RW, Rutledge G, Goldberg M. 2010. The NCEP Climate Forecast System reanalysis. Bulletin of the American Meteorological Society 91: 1015-1057. https://doi.org/10.1175/2010BAMS3001.1

Saha S, Moorthi S, Wu X, Wang J, Nadiga S, Tripp P, Behringer D, Hou Y-T, Chuang H-y, Iredell M, Ek M, Meng J, Yang R, Mendez MP, van den Dool H, Zhang Q, Wang W, Chen M, Becker E. 2014. The NCEP Cimate Forecast System version 2. Journal of Climate 27: 2185-2208. https://doi.org/10.1175/JCLI-D-12-00823.1

Salio P, Nicolini M, Zipser EJ. 2007. Mesoscale convective systems over southeastern South America and their relationship with the South American low-level jet. Monthly Weather Review 135: 1290-1309. https://doi.org/10.1175/MWR3305.1

Seluchi ME, Saulo AC, Nicolini M, Satyamurty P. 2003. The northwestern Argentinean low: A study of two typical events. Monthly Weather Review 131: 2361-2378. https://doi.org/10.1175/1520-0493(2003)131%3C2361:TNALAS%3E2.0.CO;2

Sinclair MR. 1996. A climatology of anticyclones and blocking for the Southern Hemisphere. Monthly Weather Review 124: 245-263. https://doi.org/10.1175/1520-0493(1996)124%3C0245:ACOAAB%3E2.0.CO;2

Silva Dias MAF. 2011. An increase in the number of tornado reports in Brazil. Weather, Climate, and Society 3: 209-217. https://doi.org/10.1175/2011WCAS1095.1

Simmonds I, Keay K. 2000. Mean Southern Hemisphere extratropical cyclone behavior in the 40-year NCEP-NCAR reanalysis. Journal of Climate 13: 873-885. https://doi.org/10.1175/1520-0442(2000)013%3C0873:MSHECB%3E2.0.CO;2

Taljaard JJ. 1972. Synoptic meteorology of the Southern Hemisphere. In: Meteorology of the Southern Hemisphere (Loon H, Taljaard JJ, Sasamori T, London J, Hoyt DV, Labitzke K, Newton CW., Eds.). American Meteorological Society. Meteorological Monographs 35: 139-213.

Teixeira MD, Satyamurty P. 2007. Dynamical and synoptic characteristics of heavy rainfall episodes in southern Brazil. Monthly Weather Review 135: 598-617. https://doi.org/10.1175/MWR3302.1

Velasco I, Fritsch JM. 1987. Mesoscale convective complexes in the Americas. Journal of Geophysical Research Letters: Atmospheres 92: 9591-9613. https://doi.org/10.1029/JD092iD08p09591

Zipser EJ, Cecil DJ, Liu C, Nesbitt SW, Yorty DP. 2006. Where are the most intense thunderstorms on Earth? Bulletin of the American Meteorological Society 87: 1057-1072. https://doi.org/10.1175/BAMS-87-8-1057